BIOCHEMISTRY

 Volume 46, Number 46 November 20, 2007

Articles

Thermodynamic Redox Behavior of the Heme Centers of *cbb*$_3$ Heme-Copper Oxygen Reductase from *Bradyrhizobium japonicum*†

Andreia F. Veríssimo, Filipa L. Sousa, António M. Baptista, Miguel Teixeira, and Manuela M. Pereira*

Instituto de Tecnologia Química e Biológica, Universidade Nova de Lisboa, Apartado 127, Av. da República (EAN), 2781-901 Oeiras, Portugal

Received April 18, 2007; Revised Manuscript Received September 14, 2007

ABSTRACT: A comprehensive study of the thermodynamic redox behavior of the hemes from the *cbb*$_3$ oxygen reductase from *Bradyrhizobium japonicum* was performed. This enzyme is a member of the C-type heme-copper oxygen reductase superfamily and has three subunits with six redox centers: four low-spin hemes and a high-spin heme and one copper ion, composing the site where oxygen is reduced. In this analysis, the visible spectra and redox properties of the five heme centers were deconvoluted. Their redox profiles and the pH dependence of the midpoint reduction potentials (redox-Bohr effect) were investigated. The reference reduction potentials (defined for a state where all centers are reduced) and homotropic interaction potentials were determined in the framework of a model of pairwise interacting redox centers. At pH 7.7, the reference reduction potentials for the three hemes *c* are 390, 300, and 220 mV, with low interaction potentials between them, weaker than −15 mV. For hemes *b* and b_3, reference reduction potentials of 375 and 290 mV, respectively, were obtained; these two redox centers show an interaction potential weaker than −60 mV. The midpoint reduction potentials of all five hemes are pH-dependent. The study of these thermodynamic parameters is important in understanding the coupling mechanism of the redox and chemical processes during oxygen reduction. The analysis of the thermodynamic redox behavior of the *cbb*$_3$ oxygen reductase contributes to the investigation of the mechanism of electron transfer and proton translocation by heme-copper oxygen reductases in general and indicates a thermodynamic coupling for the electron and proton transfer mechanisms.

Oxygen reductases are the terminal electron-accepting enzymes of respiratory chains, using O_2 as the final electron acceptor. These complexes catalyze the transfer of electrons to molecular oxygen, producing water with consumption of protons. Most oxygen reductases are members of the heme-copper oxygen reductase superfamily (*1*). These enzymes couple the catalytic reaction to the translocation of protons across the membrane, creating a transmembrane difference of electrochemical potential responsible for the ATP production by ATP synthase (*2*).

On the basis of sequence analyses of functional relevant amino acid residues for proton transfer (*3*), later supported by the properties of the catalytic center (*4*), the heme-copper oxygen reductase superfamily was organized into three different families, named A, B, and C (*3*). Subunit I, which harbors the catalytic center and a low-spin heme, is common to all members of this superfamily. The catalytic bimetallic center consists of a high-spin heme and a copper ion, Cu_B. A- and B-type oxygen reductases have an equivalent subunit

† This work was supported by Fundação para a Ciência e a Tecnologia: project grants (POCTI/BME/45122/2002 to M.M.P. and POCI/BIA-PRO/58608/2004 to M.T.) and fellowships (SFRH XXI/BD/14388/2003 for A.F.V. and SFRH XXI/BD/27972/2006 for F.L.S.).

* To whom correspondence should be addressed: Instituto de Tecnologia Química e Biológica, Universidade Nova de Lisboa, APT 127, Av. da República (EAN), 2781-901 OEIRAS, Portugal. Phone: 351-214469321. Fax: 351-214428314. E-mail: mpereira@itqb.unl.pt.

10.1021/bi700733g CCC: $37.00
Published on Web 10/27/2007

II, which in the case of oxygen reductases oxidizing periplasmatic metalloproteins [cytochrome *c*, high-potential iron−sulfur protein (HiPIP), or Cu proteins] contains a binuclear copper center, Cu_A. All the members of C-type family are cbb_3-type enzymes, consisting of a subunit I with the low-spin heme *b* and the binuclear oxygen reducing center heme b_3-Cu_B, and two other cytochrome *c* subunits: the monohemic subunit II and the dihemic subunit III (*3*). These mediate the transfer of electrons from soluble electron carriers to subunit I.

Oxygen reductases have been extensively studied over the last decades, and different models have been proposed for the oxygen reduction catalytic cycle and the proton pumping mechanism (*5*−*11*). However, there are still many questions to be addressed. It is not clear yet how these enzymes couple the electron transfer through the redox centers to the pumping of protons across the membrane, especially for the cbb_3 oxygen reductases, which are the less studied enzymes of this superfamily, albeit having the highest oxygen affinity (*12*). It has been shown that cbb_3 oxygen reductases are proton pumps (*13*), but the H^+/e stoichiometry must be investigated further. The D- or K-channel amino acid residues typical of the A-type enzymes are not present, and the existence of the tyrosyl covalently bound to the copper hystidyl ligand proven for the A- and B-type enzymes, and which has been considered fundamental for the catalytic reaction, is still under debate for C-type enzymes (*3*, *14*, *15*). Furthermore, these enzymes contain three extra redox heme centers. All these issues raise questions about the possibility of different coupling and/or different proton entry/gating mechanisms.

Studies concerning the thermodynamic redox behavior of a cbb_3-type oxygen reductase are first steps toward further understanding the mechanism of electron transfer and proton uptake and translocation for this subfamily of heme-copper oxygen reductases. In this study, the thermodynamic redox behavior of the five heme centers present in the cbb_3-type oxygen reductase isolated from *Bradyrhizobium japonicum* and its pH dependence (redox-Bohr effect) are investigated. It is the first time that such an exhaustive study of a member of the C-type family of heme-copper oxygen reductases has been conducted.

MATERIALS AND METHODS

Bacterial Growth and Protein Purification. B. japonicum strain Bj4639, containing the pRJ4639 plasmid in which the $FixN^{His}OQP$ operon, encoding the cbb_3 oxygen reductase, was cloned (*13*), was grown in a 30 L reactor at 28 °C, at 150 rpm and low aeration (oxygen tensions below 1%) for 5 days. Under these conditions, the FixNOQP operon was induced and the cbb_3 oxygen reductase had its expression enhanced. The enzyme was purified to homogeneity according to ref *13*, as judged by SDS−PAGE and visible spectroscopy.

Redox Titrations. Anaerobic potentiometric titrations were monitored by visible spectroscopy between 380 and 700 nm in a Shimadzu UV-1603 spectrophotometer, at 25 °C, and at several pH values in a glass cuvette with a path length of 1 cm and a working volume of 2.5 mL. Each titration was carried out using 50 mM Mes-BisTrisPropane, 10% glycerol, and 0.01% *n*-dodecyl β-D-maltoside as the buffer (adjusted to the selected pH value), 1.5 μM purified cbb_3 oxygen reductase, and the following redox mediators at a final concentration of 15 μM: ferrocenecarboxylic acid, potassium ferricyanide, *N*,*N*-dimethyl-*p*-phenylenediamine, *p*-benzoquinone, 1,2-naphthoquinone-4-sulfonic acid, 1,2-naphthoquinone, trimethylhydroquinone, phenazine methosulfate, 1,4-naphthoquinone, duroquinone, and menadione. The cuvette was home-adapted to ensure an anaerobic environment during the titration process. The cuvette and sample were flushed with argon before and during the titration, and the sample was continuously stirred to produce a homogeneous solution. Sodium dithionite was used as a reductant and potassium hexachloroiridate (IV) as an oxidant. Reductive and oxidative solutions were prepared in 250 mM Tris-HCl (pH 8.7) and 100 mM Tris-HCl (pH 7.5), respectively, and made anaerobic by being degassed and flushed with argon. These solutions were kept under an argon atmosphere during the titration. Small additions were made with a 10 μL gastight Hamilton syringe to yield 5−10 mV oxidation/reduction steps. A combined silver/silver chloride electrode was used, calibrated with a saturated quinhydrone solution at pH 7.0 and 25 °C. The reduction potentials were quoted versus the standard hydrogen electrode.

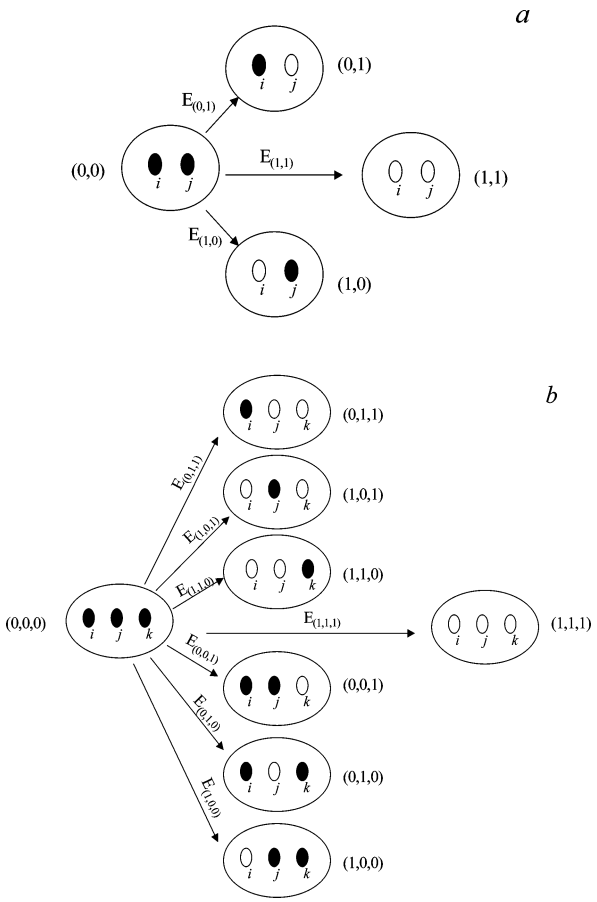

FIGURE 1: Schematic representation of the transitions between the reference (fully reduced) microstate and each of the other partially or fully oxidized microstates for a two-redox center (a) and three-redox center (b) system. The reduction potentials shown are the ones following a Nernst equation (eq 1). The white ovals represent oxidized centers and the black ovals reduced centers.

Data Analysis. Visible spectra were measured from 380 to 700 nm at each reduction potential. The data were analyzed using MATLAB (Math Works). Due to the strong overlap of the different hemes at the Soret region, the analysis

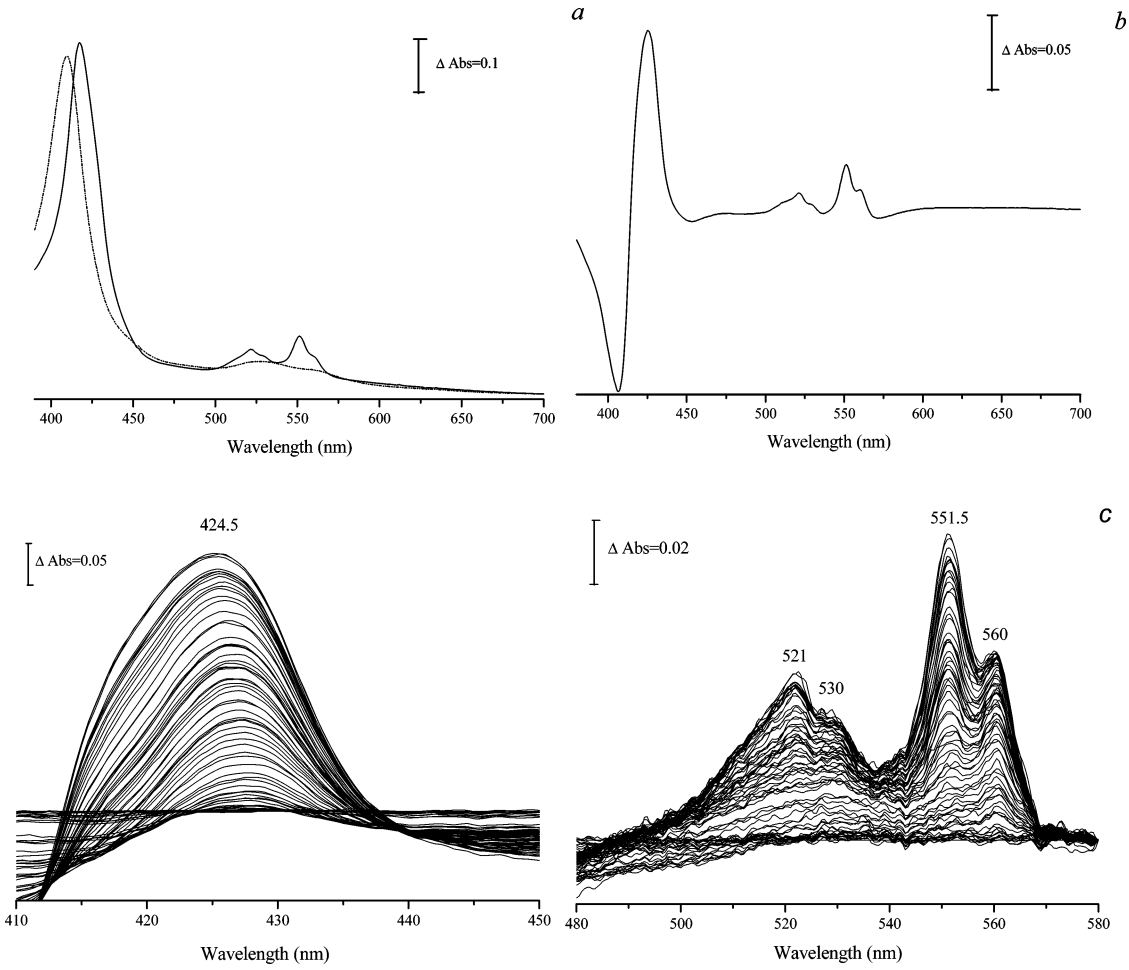

FIGURE 2: (a) Visible spectra of the oxidized (···) and dithionite-reduced (—) *cbb*$_3$ oxygen reductase from *B. japonicum*. (b) Difference between the spectrum of the reduced *cbb*$_3$ enzyme and the spectrum of the oxidized enzyme. (c) Difference between the spectra of the reduced *cbb*$_3$ oxygen reductase upon successive additions of sodium dithionite and the spectrum of the fully oxidized enzyme. The difference spectra were obtained during the redox titration of the enzyme from 522 to 0 mV, at pH 7.7.

was focused mainly at the α-band region, which allowed the deconvolution of the different heme centers by inspection of the individual spectra or by means of successive subtractions. Once all optical components were identified and deconvoluted, the changes in absorbance at the corresponding maxima at the α-band region (551.5 and 560 nm for C- and B-type hemes, respectively) as a function of the solution reduction potential were used to determine the redox transitions of each heme center. The data collected were fit in the framework of a model of pairwise interacting redox centers, which describes the thermodynamic behavior of the system. In this model, a system with N redox centers has 2^N different redox microstates, each of which can be represented by a vector $\mathbf{a} = (a_1, a_2, ..., a_N)$, where $a_i = 0$ or 1 depending on whether center i is reduced or oxidized, respectively. When the state populations are related to each other, it is convenient to consider a reference microstate, which will be taken here as the fully reduced state $\mathbf{0} = (0, 0, ..., 0)$. The $\mathbf{a} \rightarrow \mathbf{0}$ reduction reaction involves the capture of $n_a = \sum_i a_i$ electrons, having an associated reduction potential given by the Nernst equation

$$E_a = E + \frac{RT}{n_a F} \ln \frac{P(\mathbf{0})}{P(\mathbf{a})} \quad (1)$$

where $P(\mathbf{a})$ is the probability of state $\mathbf{a}$. Rearranging terms, we obtain

$$P(\mathbf{a}) = \exp[n_a F(E - E_a)/RT]/Q \quad (2)$$

where the condition $\sum_{\mathbf{a}} P(\mathbf{a}) = 1$ (assuming that the sum extends over all the 2^N microstates) is here taken into account by introducing the normalization constant

$$Q = \sum_{\mathbf{a}} \exp[n_a F(E - E_a)/RT] \quad (3)$$

Given the probabilities $P(\mathbf{a})$, a typical macroscopically measurable redox property X_{macro} can be easily expressed as the average of its microscopic (molecular) counterpart $X_{\mathbf{a}}$:

$$X_{\text{macro}} = \overline{X_{\mathbf{a}}} = \sum_{\mathbf{a}} X_{\mathbf{a}} P(\mathbf{a}) \quad (4)$$

For example, the oxidation probability of the whole system is

$$\overline{\frac{n_a}{N}} = \sum_a \frac{n_a}{N} P(\mathbf{a}) = \frac{1}{N} \sum_a \sum_i a_i P(\mathbf{a}) = \frac{1}{N} \sum_i \sum_a a_i P(\mathbf{a}) = \frac{1}{N} \sum_i \overline{a_i} \quad (5)$$

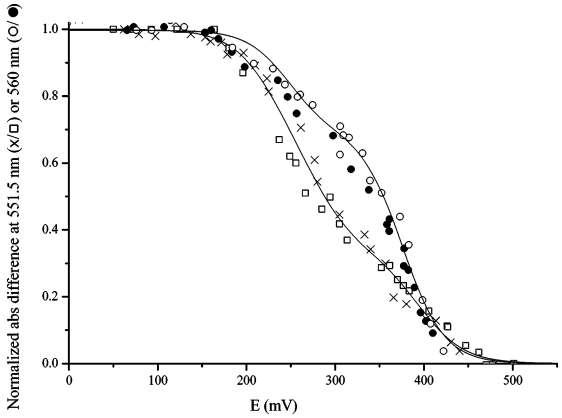

FIGURE 3: Changes in absorbance as a function of the solution reduction potential obtained for the *cbb*$_3$ oxygen reductase at pH 7.14 during reductive and oxidative redox titrations. Data were collected at α-band maxima, 551.5 nm [(×) reductive and (□) oxidative] and 560 nm [(○) reductive and (●) oxidative], for *c*- and *b*-type hemes, respectively.

where

$$\overline{a_i} = \sum_a a_i P(\mathbf{a}) \tag{6}$$

is the oxidation probability of center *i* (i.e., the probability of center *i* in the oxidized form).

A pairwise interaction model may be introduced by assuming that all the E_a reduction potentials can be written as

$$E_a = \sum_i a_i e_i - \sum_{i>j} a_i a_j I_{ij} \tag{7}$$

If we consider a vector where $a_i = 1$ and all $a_{i\neq j} = 0$, it is easy to see that e_i is the reduction potential of center *i* when all other centers remain in the reference (reduced) state; thus, e_i may be called the reference reduction potential of site *i*. Sometimes, this e_i is called the low asymptotic value of the midpoint potential. The term I_{ij} can be regarded as the interaction between centers *i* and *j*, with a positive or negative signal indicating a cooperative or anticooperative effect between the centers, respectively. This term does not represent a mere Coulombic electrostatic interaction, since it also reflects changes in all properties of the system not explicitly included in the model, such as conformational changes, changes in the oxidation state of other redox groups, and also protonation/deprotonation reactions of protolytic groups; in other words, each I_{ij} is a free energy. A different reference state can be chosen (e.g., the fully oxidized state), but the physical meaning of e_i and I_{ij} has to be changed accordingly.

In the particular case where $I = 0$, this model implies the situation equivalent to the sum of individual Nernst curves.

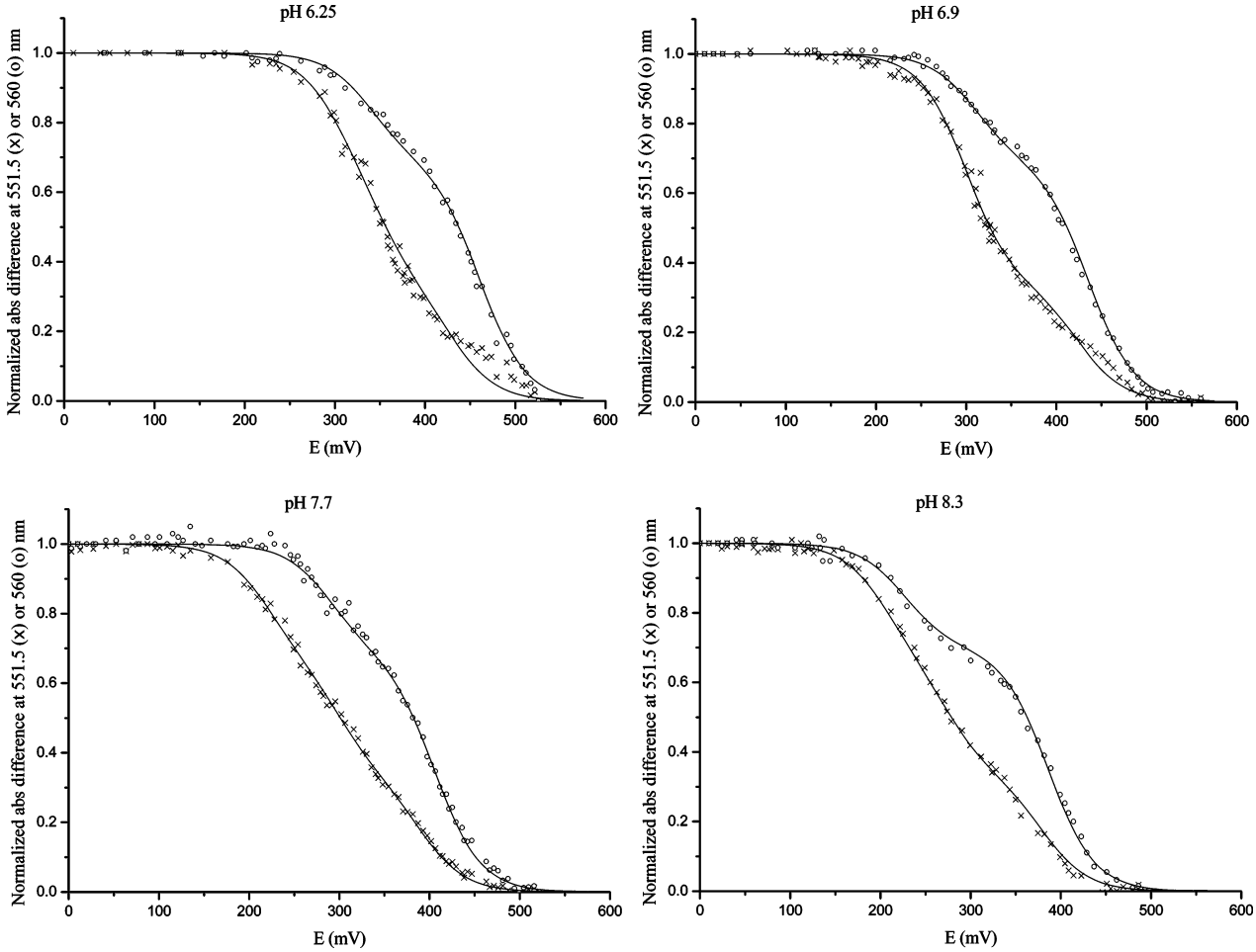

FIGURE 4: Reductive redox titration curves obtained for *B. japonicum cbb*$_3$ oxygen reductase at pH 6.25, 6.9, 7.7, and 8.3. Data were collected at α-band maxima, 551.5 (×) and 560 nm (○). Solid lines are the best fits obtained by the model of three interacting centers for the *c*-type hemes and by the model of two interacting redox centers for the b_3- and *b*-type hemes. The reference reduction potentials obtained for each redox titration are summarized in Table 1.

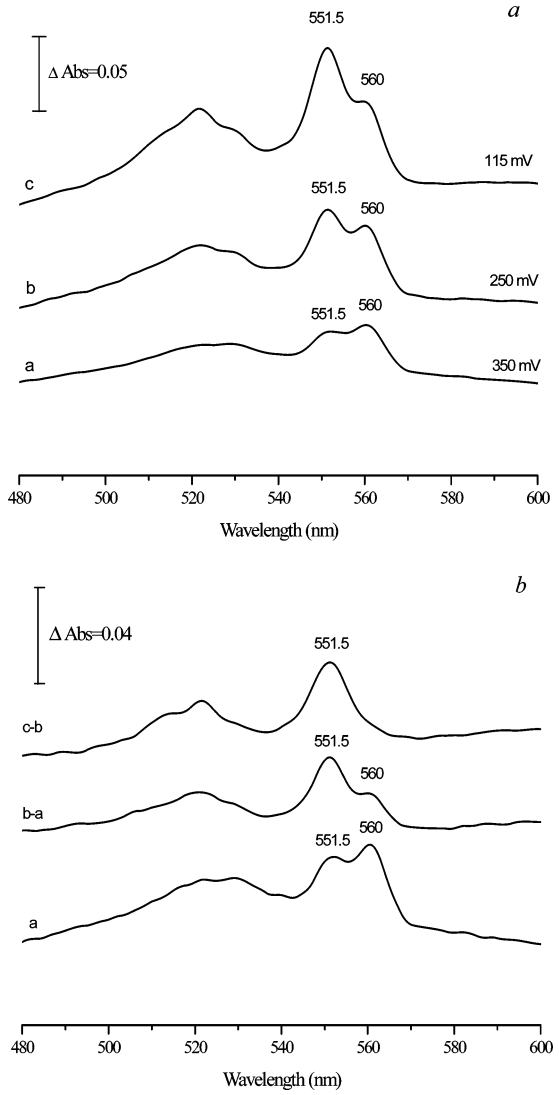

FIGURE 5: (a) Difference between the spectra of the partially reduced *cbb*$_3$ oxygen reductase at 350 (a), 250 (b), and 150 mV (c) and the spectrum of the fully oxidized enzyme, obtained for the titration at pH 7.7. (b) Difference between the spectrum of the partially reduced enzyme at 350 mV and the spectrum of the oxidized enzyme (a). Difference between the spectra of the partially reduced enzyme at 350 and 250 mV (b-a). Difference between the spectra of the partially reduced enzyme at 250 and 150 mV (c-b).

Given some experimentally measured quantities, X_{macro}, Y_{macro}, Z_{macro}, ..., we can find the set of e_i and I_{ij} values that gives the optimal fit between those quantities and the computed $\overline{X_a}$, $\overline{Y_a}$, $\overline{Z_a}$, ... That set corresponds to the pairwise model that better describes the experimental data. In particular, the experimental quantities may be the values defining one or several *E*-dependent properties (e.g., they may be the points of one or several reduction curves).

In the absence of structural data, the localization of the five hemes is not known; it was chosen to consider the C- and B-type hemes separately. For the B-type hemes, located in subunit I, we applied a model of two interacting centers (Figure 1a). For the C-type hemes, located on subunits II and III, we applied a model of three interacting centers (Figure 1b).

The fit of the heme B species data took into account the difference between the molar absorption coefficients of a low- and high-spin cytochrome *b*. As an approximation of molar absorption coefficients, the ones from horse heart myoglobin, a high-spin cytochrome *b* (13.8 mM^{-1} cm^{-1}) (*16*), and from *Escherichia coli* cytochrome b_{562}, a low-spin heme-containing protein (32 mM^{-1} cm^{-1}) (*17*, *18*), were used. The three C-type hemes were considered to have equal molar absorption coefficients at the respective α-bands.

Table 1: Reference Reduction Potentials and Interaction Potentials Obtained for the Five Heme Centers at Different pH Values

pH	e_{CH} (mV)	e_{CM} (mV)	e_{CL} (mV)	$I_{CHCM}/I_{CMCL}/I_{CHCL}$ (mV) (weaker than)	e_B (mV)	e_{B3} (mV)	I_{BB3} (mV) (mean value)
6.15	430	335	290	−15	420	310	−30
6.25	420	350	300	−15	430	340	−30
6.90	415	320	280	−15	405	310	−30
7.14	400	300	230	−15	395	275	−30
7.70	390	300	220	−15	375	290	−30
7.90	395	290	190	−15	385	280	−30
8.30	375	280	210	−15	355	225	−30

As discussed above, the parameters e_i and I_{ij} are determined as those giving the best fit to the measured populations. Once the parameters are obtained, it is possible to calculate the populations of all microstates as a function of the solution reduction potential. From these populations, the oxidized and reduced fractions of the centers can be determined, as well as their midpoint reduction potentials. The midpoint reduction potential of each redox center was determined as the *E* value at which half of the center *i* population is reduced.

The equilibrium constant that describes the electron transfer between two centers is given by

$$K_{eq} = P(a_i=0,a_j=1)/P(a_i=1,a_j=0) \quad (8)$$

To obtain better visual guidance for the pH dependence of the heme center midpoint reduction potentials, straight lines (without physical meaning) were adjusted to the data points in Figure 7.

RESULTS AND DISCUSSION

Several redox titrations of the *cbb*$_3$ oxygen reductase were carried out at different pH values, monitored by visible spectroscopy between 380 and 700 nm, to obtain a general description of the reductive profile of the enzyme. The difference between the spectrum of the reduced protein and the spectrum of the oxidized protein shows a broad maximum at 424.5 nm (Soret band), and α-bands at 551.5 and 560 nm corresponding to hemes *c* and *b*, respectively (Figure 2).

Due to the large spectral overlap at the Soret region, as expected for *b*- and *c*-type hemes, the analysis was mainly focused on the α-bands, and a complete deconvolution of the redox properties was performed on the basis of this spectral region. The data were analyzed by monitoring the absorbance changes at 551.5 and 560 nm (Figures 2 and 3), as a function of the solution reduction potential.

The redox titrations were fully reversible as exemplified by the profiles presented in Figure 3; in Figure 4, several reductive titrations are presented. The appropriateness of the chosen wavelengths to follow the reduction of *c*- and *b*-type hemes was corroborated by the spectral deconvolution shown in Figure 5. Three redox transitions were observed (Figure 5a,b). The first corresponds to the reduction of *c*- and *b*-type hemes (Figure 5b, spectrum a). In the second, also *c*- and *b*-type hemes are reduced (Figure 5b, spectrum b − a). In

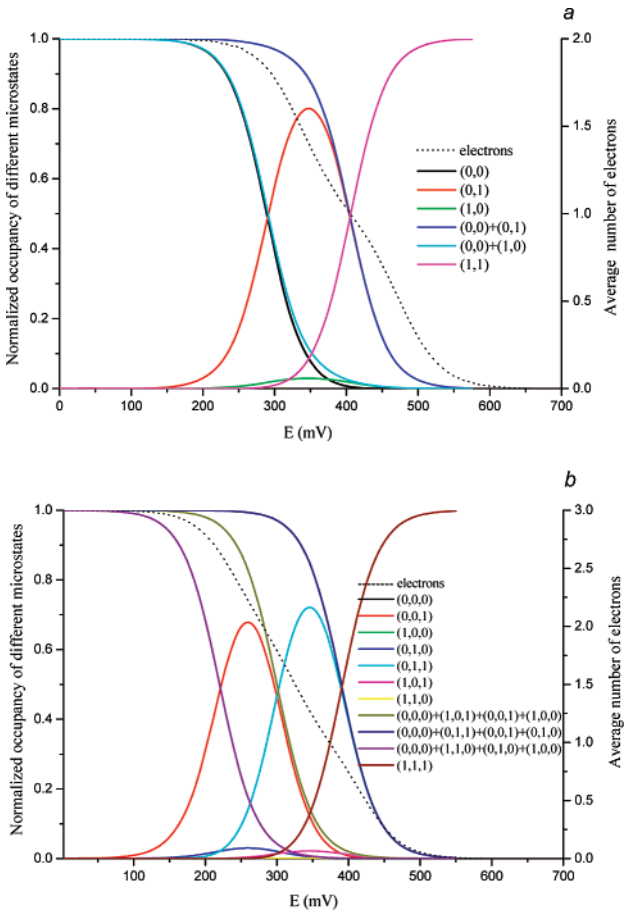

FIGURE 6: Relative occupancies of the different microstates at pH 7.7 and average number of electrons involved. Microstate probabilities were defined by the model of two interacting centers (a) and by the model of three interacting centers (b) used to describe the reductive profile of hemes *b* and *c*, respectively.

Table 2: Relative Occupancies of the Different Microstates When the Total Average Number of Electrons Loaded on Heme *b* Species Is 1, at Different pH Values, According to the Model of Two Interacting Redox Centers[a]

pH	(1,1) (%)	(1,0) (%)	(0,1) (%)	(0,0) (%)
6.15	5.7	1.2	87.4	5.7
6.25	7.9	2.5	81.7	7.9
6.90	6.6	2.0	83.3	8.1
7.14	4.8	0.9	89.5	4.8
7.70	7.7	2.9	80.0	9.4
7.90	5.6	1.4	86.2	6.8
8.30	3.3	0.6	91.2	4.9

[a] Microstates are shown as (a_b,a_{b_3}).

the third, only the reduction of *c*-type hemes is observed (Figure 5b, spectrum c − b). Furthermore, it can be observed from Figure 5 that spectral overlapping of the different heme types is negligible at the chosen wavelengths.

Reference reduction potentials were determined using the model for pairwise interacting redox centers. For the three *c*-type hemes, located at subunits II and III, a model of three interacting redox centers (Figure 1b) was applied. Although the relative locations of the *c*-type hemes is not known, we assumed that they are sufficiently close to experience homotropic cooperativities between them, since all these redox centers are probably involved in transfer of electrons to subunit I. Electrostatic interactions between hemes *c* and

Table 3: Percentage of Reduction of Hemes *b* and b_3 When the Total Average Number of Electrons Loaded on These Hemes Is 1, at Different pH Values, According to the Model of Two Interacting Redox Centers[a]

pH	$E_{half-red}$ (mV)	heme *b* reduced (%) (0,0) + (0,1)	heme b_3 reduced (%) (0,0) + (1,0)
6.15	450	93.1	6.9
6.25	460	89.6	10.4
6.90	435	91.3	10.1
7.14	425	94.3	5.7
7.70	405	89.3	12.3
7.90	415	92.9	8.3
8.30	385	96.2	5.9

[a] Microstates are shown as (a_b,a_{b_3}).

Table 4: Relative Occupancies of the Different Microstates When the Total Average Number of Electrons Loaded on Heme *c* Species Is 1.5, at Different pH Values, According to the Model of Three Interacting Redox Centers[a]

pH	(1,1,1) (%)	(1,1,0) (%)	(1,0,1) (%)	(0,1,1) (%)	(0,1,0) (%)	(1,0,0) (%)	(0,0,1) (%)	(0,0,0) (%)
6.15	1.7	0.2	1.2	49.5	6.3	0.1	36.4	4.6
6.25	3.4	0.4	2.9	44.7	5.4	0.3	38.2	4.7
6.90	1.7	0.2	1.2	49.3	7.3	0.2	34.9	5.2
7.14	1.2	0.1	0.9	48.9	2.8	0.1	43.5	2.5
7.70	1.5	0.1	1.4	47.4	2.0	0.1	45.6	1.9
7.90	0.8	0.1	0.7	48.2	1.0	0.1	48.1	1.0
8.30	1.4	0.1	1.2	48.6	2.8	0.1	43.3	2.5

[a] Microstates are shown as $(a_{c_H},a_{c_M},a_{c_L})$.

b were not accounted for. On the basis of a putative resemblance between the location of the monohemic and dihemic subunits with respect to subunit I and that of subunit II for A- and B-type enzymes, hemes *c* and *b* were considered to be located at least 20 Å apart. Given the amino acid sequence comparisons, as well as the available three-dimensional models (*14*, *15*), the *b*-type hemes, located in subunit I, should be located at the same distances as in A- or B-type enzymes, i.e., at 13−14 Å (*19*, *20*), distances at which electrostatic interactions may be relevant. In this case, we applied a model of two interacting redox centers (Figure 1a).

In the catalytic subunit I, there is still a third redox entity, the copper center Cu_B that together with the high-spin heme b_3 constitutes the catalytic oxygen reducing binuclear site. In this case, a model of three interacting redox centers should be applied, with three reduction potentials and three interaction potentials as variables. However, the redox profile of the Cu_B center could not be monitored by visible spectroscopy, and it would be completely arbitrary to assign any value to the reduction potential of Cu_B, as well as to the interaction between this center and each of the hemes. Recent studies performed with the aa_3 oxygen reductase from *Paracoccus denitrificans*, an A-type enzyme, have shown that the redox behavior of the two heme centers in subunit I can be described without taking into account Cu_B (*21*).

At pH 7.7, the reference reduction potentials for the *c*-type hemes are 390, 300, and 220 mV, with small interaction potentials, weaker than −15 mV. The three *c*-type hemes were named c_H, c_M, and c_L, which stand for high-, medium-, and low- potential *c*-type hemes, respectively.

For the *b*-type hemes, reference reduction potentials of 375 and 290 mV were determined at the same pH value.

Table 5: Percentage of Reduction of Hemes c_H, c_M, and c_L When the Total Average Number of Electrons Loaded on These Hemes Is 1.5, at Different pH Values, According to the Model of Three Interacting Redox Centers[a]

pH	$E_{half\ -red}$ (mV)	heme c_H reduced (%) (0,0,0) + (0,1,1) + (0,0,1) + (0,1,0)	heme c_M reduced (%) (0,0,0) + (1,0,1) + (0,0,1) + (1,0,0)	heme c_L reduced (%) (0,0,0) + (1,0,1) + (0,1,0) + (1,0,0)
6.15	345	96.7	42.3	11.2
6.25	355	92.9	46.1	10.9
6.90	330	96.6	41.3	12.9
7.14	305	97.7	47.1	5.5
7.70	300	96.9	49.0	4.1
7.90	290	98.4	50.0	2.0
8.30	285	97.3	47.1	5.5

[a] Microstates are shown as (a_{c_H},a_{c_M},a_{c_L}).

Table 6: Midpoint Reduction Potentials and Joint Half-Reduction Potentials ($E_{half-red}$) for *c* and *b* Heme Centers at Different pH Values

pH	E_{c_H} (mV)	E_{c_M} (mV)	E_{c_L} (mV)	$E_{half-red}$ (mV)	E_b (mV)	E_{b_3} (mV)	$E_{half-red}$ (mV)
6.15	430	335	290	345	450	310	380
6.25	420	350	300	355	460	340	400
6.90	415	320	280	330	435	310	370
7.14	400	300	230	305	425	275	350
7.70	390	300	220	300	405	290	345
7.90	395	290	190	290	415	280	345
8.30	375	280	210	285	385	225	300

The difference in the molar absorption coefficient for hemes *b* and b_3 was taken into account in the fit, meaning that the first reference reduction potential can now be attributed to low-spin heme *b* and the second to high-spin heme b_3. The fits were equally good using interaction parameters in the range of −60 to 0 mV. Thus, an interaction between the heme groups of the *cbb*$_3$ enzyme may not be present, but its presence cannot be neglected. As mentioned in Materials and Methods, in the particular case where $I = 0$, this model implies the situation equivalent to the sum of individual Nernst curves.

The results obtained at different pH values are summarized in Table 1. The reference reduction potentials determined are within the range of those reported in preliminary studies for the *Pseudomonas stutzeri* (*22*) and *Rhodobacter capsulatus* (*23*) *cbb*$_3$ enzymes.

The model-derived populations of the four microstates of heme *b* species, as well as the number of uptaken electrons, are shown for pH 7.7 in Figure 6a and Tables 2 and 3. It can be observed that when the average number of total electrons taken up by both heme *b* species is one (i.e., at their joint half-reduction), there are different contributions from each heme (Table 3). It is shown that it is the low-spin heme *b* that is predominantly reduced at this stage, or in other words, that the hemes have quite different reduction potentials with a transfer equilibrium constant of 27, and that the reduction potential of low-spin heme *b* is higher than that of high-spin heme b_3. Thus, the α-band with a maximum at 560 nm present in spectrum a of Figure 5 is assigned to heme *b*, while the α-band with a maximum at 560 nm present in spectrum b − a corresponds to heme b_3. Figure 6b and Tables 4 and 5 describe the relative occupancies of the eight possible microstates of the three heme *c* species and the number of electrons taken up at the same pH. It is observed that at the joint half-reduction of the three heme *c* forms, approximately at 300 mV, both microstates $\mathbf{a} = (0,1,1)$ and $\mathbf{a} = (0,0,1)$, containing only the C_H or the C_H and C_M reduced, are the most populated and equally probable.

The electron affinity of a redox center can depend on the protonation state of acidic/basic group(s), the proton affinities (pK_a) of which can change according to the oxidation state of that center, what is generally called the redox-Bohr effect (*6*, *24*−*26*), a heterotropic (proton−electron) interaction. Homo- and heterotropic cooperativities between redox and protonatable centers have already been suggested and reported for oxygen reductases (*21*, *27*−*31*), showing that they play an important role in the overall functional mechanism. This pH dependence is here characterized using the midpoint reduction potential of each heme. This quantity is given by the solution potential for which that heme is half-reduced, meaning the solution potential at which the heme is most frequently exchanging electrons, information not provided by the reference reduction potentials derived from the model. The midpoint reduction potentials of all heme centers are pH-dependent in the physiological pH range (Figure 7 and Table 6). The pH dependencies of the midpoint reduction potentials for hemes *b* and b_3 are, approximately, −30 and −37 mV/pH unit, respectively, in the studied pH range. For the *c*-type hemes, the three midpoint potentials were assigned to heme c_H, c_M, and c_L, corresponding to the hemes having the highest, medium, and lowest reference reduction potential, respectively. However, at least in the case of c_M and c_L, they cannot be assured to correspond to the same heme at all pH values. Two of the heme *c* forms have weak pH dependence, approximately −23 and −29 mV/pH unit, whereas the other one has a stronger pH dependence of −49 mV/pH unit.

As mentioned in the data analysis description in Materials and Methods, the straight lines shown in Figure 7 are just intended to help in the visualization of the change in the midpoint reduction potentials at different pH values. There were no attempts to relate the pH dependence of the midpoint reduction potentials with the effect of protonatable groups by means of the equation

$$E = E_{acid} + \frac{RT}{F}\ln\left(\frac{K_{Red} + [H^+]}{K_{Ox} + [H^+]}\right)$$

Although of widespread use, this equation holds only in the case where a single redox center is under the influence of a unique protonatable center that undergoes only one ionization, which is not the case in large multiredox center proteins, such as heme-copper oxygen reductases. In these

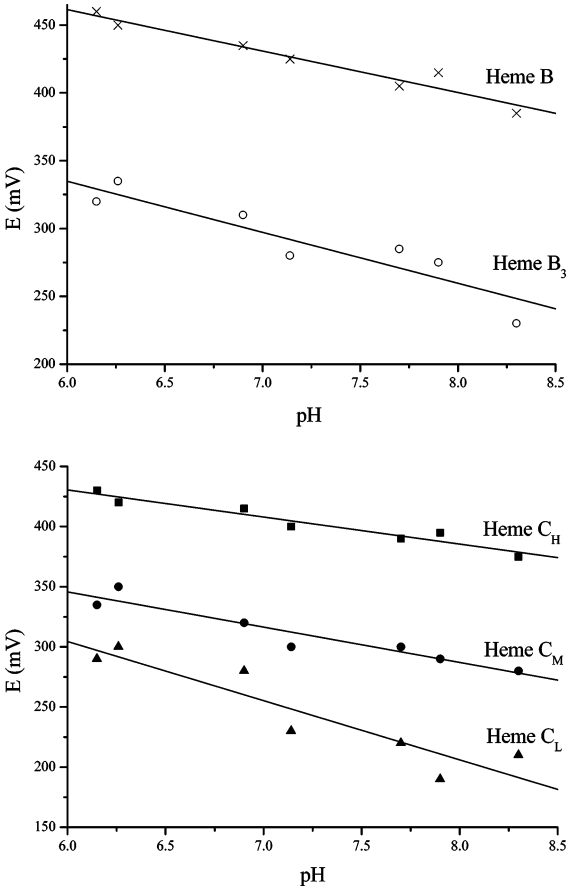

FIGURE 7: pH dependence of the midpoint reduction potentials of the heme centers of the cbb_3 oxygen reductase from *B. japonicum*: hemes *b* (×), b_3 (○), c_H (■), c_M (●), and c_L (▲) (high, medium, and low midpoint reduction potentials, respectively). Straight lines were adjusted to the experimental data to help in the visualization of the pH dependence of the midpoint reduction potentials for all the hemes.

enzymes, there is more than a single redox center present, and certainly each one is influenced by several protonatable sites, as clearly shown by multiple theoretical studies (*32*−*36*). Applying this equation to oxygen reductases will lead to the determination of pK_{ox} and pK_{red} without precise microscopic meaning, and clearly not attributable to a single protonatable group.

The redox behavior observed for *B. japonicum* cbb_3 oxygen reductase differs from that described so far for bovine (*30*, *37*, *38*) and *P. denitrificans* enzymes (*21*) (A-type), in the sense that the heme *b* species present in subunit I show a considerable difference between their reduction potentials. The studies described for these two A-type enzymes indicate that the hemes have similar reduction potentials and thus each loaded electron equilibrates equally between the two hemes (*21*, *30*, *37*, *38*). The pH dependence of the midpoint reduction potential of the hemes strongly indicates a thermodynamic linkage between at least some of the steps of the catalytic and proton uptake mechanisms, possibly important for proton translocation. The fact that the *c*-type hemes also have a non-negligible pH dependence of the midpoint reduction potentials, which may appear irrelevant since those are most probably extrinsic to the membrane and facing the periplasm, may be quite important if localized proton circuits are operative in energy transduction (*39*).

This was the first time that an exhaustive study of the thermodynamic redox behavior of a member of the C-type family was performed. A large difference in the midpoint reduction potentials of both hemes *b* and b_3 present in subunit I was observed, which is in contrast to the reports for the A1-type enzymes for which similar reduction potentials for both hemes were proposed (*21*, *30*, *37*, *38*). These findings may have implications in the catalytic mechanism of C-type enzymes and in the coupling between electron transfer and proton translocation.

ACKNOWLEDGMENT

João Carita and Sara Baptista are acknowledged for cell growth and protein purification. Dr. Hans Martin Fisher is acknowledged for the kind gift of *B. japonicum* strain Bj4639 and for the helpful discussions concerning the optimization of growth conditions.

REFERENCES

1. Garcia-Horsman, J. A., Barquera, B., Rumbley, J., Ma, J., and Gennis, R. B. (1994) The superfamily of heme-copper respiratory oxidases, *J. Bacteriol. 176*, 5587−5600.
2. Wikstrom, M. K. (1977) Proton pump coupled to cytochrome c oxidase in mitochondria, *Nature 266*, 271−273.
3. Pereira, M. M., Santana, M., and Teixeira, M. (2001) A novel scenario for the evolution of haem-copper oxygen reductases, *Biochim. Biophys. Acta 1505*, 185−208.
4. Pereira, M. M., and Teixeira, M. (2004) Proton pathways, ligand binding and dynamics of the catalytic site in haem-copper oxygen reductases: A comparison between the three families, *Biochim. Biophys. Acta 1655*, 340−346.
5. Michel, H. (1999) Cytochrome c oxidase: Catalytic cycle and mechanisms of proton pumping-a discussion, *Biochemistry 38*, 15129−15140.
6. Xavier, A. V. (2004) Thermodynamic and choreographic constraints for energy transduction by cytochrome c oxidase, *Biochim. Biophys. Acta 1658*, 23−30.
7. Wikstrom, M. (2004) Cytochrome c oxidase: 25 years of the elusive proton pump, *Biochim. Biophys. Acta 1655*, 241−247.
8. Yoshikawa, S., Muramoto, K., Shinzawa-Itoh, K., Aoyama, H., Tsukihara, T., Ogura, T., Shimokata, K., Katayama, Y., and Shimada, H. (2006) Reaction mechanism of bovine heart cytochrome c oxidase, *Biochim. Biophys. Acta 1757*, 395−400.
9. Artzatbanov, V. Y., Konstantinov, A. A., and Skulachev, V. P. (1978) Involvement of intramitochondrial protons in redox reactions of cytochrome α, *FEBS Lett. 87*, 180−185.
10. Mitchell, P. (1988) Possible protonmotive osmochemistry in cytochrome oxidase, *Ann. N.Y. Acad. Sci. 550*, 185−198.
11. Rich, P. R. (1995) Towards an understanding of the chemistry of oxygen reduction and proton translocation in the iron-copper respiratory oxidases, *Aust. J. Plant Physiol. 22*, 479−486.
12. Preisig, O., Zufferey, R., Thony-Meyer, L., Appleby, C. A., and Hennecke, H. (1996) A high-affinity cbb3-type cytochrome oxidase terminates the symbiosis-specific respiratory chain of *Bradyrhizobium japonicum*, *J. Bacteriol. 178*, 1532−1538.
13. Arslan, E., Kannt, A., Thony-Meyer, L., and Hennecke, H. (2000) The symbiotically essential cbb_3-type oxidase of *Bradyrhizobium japonicum* is a proton pump, *FEBS Lett. 470*, 7−10.
14. Sharma, V., Puustinen, A., Wikstrom, M., and Laakkonen, L. (2006) Sequence analysis of the cbb3 oxidases and an atomic model for the *Rhodobacter sphaeroides* enzyme, *Biochemistry 45*, 5754−5765.
15. Hemp, J., Christian, C., Barquera, B., Gennis, R. B., and Martinez, T. J. (2005) Helix switching of a key active-site residue in the cytochrome cbb3 oxidases, *Biochemistry 44*, 10766−10775.
16. Wood, P. M. (1984) Bacterial proteins with CO-binding b- or c-type haem. Functions and absorption spectroscopy, *Biochim. Biophys. Acta 768*, 293−317.
17. Hay, S., and Wydrzynski, T. (2005) Conversion of the *Escherichia coli* cytochrome b562 to an archetype cytochrome b: A mutant with bis-histidine ligation of heme iron, *Biochemistry 44*, 431−439.

18. Itagaki, E., and Hager, L. P. (1966) Studies on cytochrome b-562 of *Escherichia coli*. I. Purification and crystallization of cytochrome b-562, *J. Biol. Chem. 241*, 3687−3695.
19. Soulimane, T., Buse, G., Bourenkov, G. P., Bartunik, H. D., Huber, R., and Than, M. E. (2000) Structure and mechanism of the aberrant ba(3)-cytochrome c oxidase from *Thermus thermophilus*, *EMBO J. 19*, 1766−1776.
20. Iwata, S., Ostermeier, C., Ludwig, B., and Michel, H. (1995) Structure at 2.8 Å resolution of cytochrome c oxidase from *Paracoccus denitrificans*, *Nature 376*, 660−669.
21. Gorbikova, E. A., Vuorilehto, K., Wikstrom, M., and Verkhovsky, M. I. (2006) Redox titration of all electron carriers of cytochrome c oxidase by Fourier transform infrared spectroscopy, *Biochemistry 45*, 5641−5649.
22. Pitcher, R. S., and Watmough, N. J. (2004) The bacterial cytochrome cbb3 oxidases, *Biochim. Biophys. Acta 1655*, 388−399.
23. Gray, K. A., Grooms, M., Myllykallio, H., Moomaw, C., Slaughter, C., and Daldal, F. (1994) Rhodobacter capsulatus contains a novel cb-type cytochrome c oxidase without a CuA center, *Biochemistry 33*, 3120−3127.
24. Papa, S. (1976) Proton translocation reactions in the respiratory chains, *Biochim. Biophys. Acta 456*, 39−84.
25. Xavier, A. V. (2002) A mechano-chemical model for energy transduction in cytochrome c oxidase: The work of a Maxwell's god, *FEBS Lett. 532*, 261−266.
26. Wyman, J. (1968) Regulation in macromolecules as illustrated by haemoglobin, *Q. Rev. Biophys. 1*, 35−80.
27. Verkhovsky, M. I., Morgan, J. E., and Wikstrom, M. (1995) Control of electron delivery to the oxygen reduction site of cytochrome c oxidase: A role for protons, *Biochemistry 34*, 7483−7491.
28. Salerno, J. C., Bolgiano, B., Poole, R. K., Gennis, R. B., and Ingledew, W. J. (1990) Heme-copper and heme-heme interactions in the cytochrome bo-containing quinol oxidase of *Escherichia coli*, *J. Biol. Chem. 265*, 4364−4368.
29. Moody, A. J., and Rich, P. R. (1990) The effect of pH on redox titrations of haem a in cyanide-liganded cytochrome-c oxidase: Experimental and modelling studies, *Biochim. Biophys. Acta 1015*, 205−215.
30. Babcock, G. T., Vickery, L. E., and Palmer, G. (1978) The electronic state of heme in cytochrome oxidase II. Oxidation-reduction potential interactions and heme iron spin state behavior observed in reductive titrations, *J. Biol. Chem. 253*, 2400−2411.
31. Capitanio, N., Vygodina, T. V., Capitanio, G., Konstantinov, A. A., Nicholls, P., and Papa, S. (1997) Redox-linked protolytic reactions in soluble cytochrome-c oxidase from beef-heart mitochondria: Redox Bohr effects, *Biochim. Biophys. Acta 1318*, 255−265.
32. Popovic, D. M., and Stuchebrukhov, A. A. (2004) Electrostatic study of the proton pumping mechanism in bovine heart cytochrome C oxidase, *J. Am. Chem. Soc. 126*, 1858−1871.
33. Popovic, D. M., Quenneville, J., and Stuchebrukhov, A. A. (2005) DFT/electrostatic calculations of pK_a values in cytochrome c oxidase, *J. Phys. Chem. B 109*, 3616−3626.
34. Quenneville, J., Popovic, D. M., and Stuchebrukhov, A. A. (2006) Combined DFT and electrostatics study of the proton pumping mechanism in cytochrome c oxidase, *Biochim. Biophys. Acta 1757*, 1035−1046.
35. Kannt, A., Lancaster, C. R., and Michel, H. (1998) The coupling of electron transfer and proton translocation: Electrostatic calculations on *Paracoccus denitrificans* cytochrome c oxidase, *Biophys. J. 74*, 708−721.
36. Soares, C. M., Baptista, A. M., Pereira, M. M., and Teixeira, M. (2004) Investigation of protonatable residues in *Rhodothermus marinus* caa3 haem-copper oxygen reductase: Comparison with *Paracoccus denitrificans* aa3 haem-copper oxygen reductase, *J. Biol. Inorg. Chem. 9*, 124−134.
37. Wikstrom, K. F., Harmon, H. J., Ingledew, W. J., and Chance, B. (1976) A re-avaluation of the spectral, potentiometric and energy-linked properties of cytochrome c oxidase in mitochondria, *FEBS Lett. 65*, 259−277.
38. Nicholls, P., and Petersen, L. C. (1974) Haem-haem interactions in cytochrome aa3 during the anaerobic-aerobic transition, *Biochim. Biophys. Acta 357*, 462−467.
39. Mulkidjanian, A. Y., Heberle, J., and Cherepanov, D. A. (2006) Protons @ interfaces: Implications for biological energy conversion, *Biochim. Biophys. Acta 1757*, 913−930.

BI700733G